Theoretical investigation of optical properties of optimal architectures of magnetoplasmonic nanoparticles in human tissue for potential applications in photothermal therapy

Maha Hadded, Abdelhamid Hmima, Thomas Maurer, A Chehaidar, Jerome Plain

Optical Materials 114 (2021) 110946

Contents lists available at ScienceDirect

Optical Materials

journal homepage: http://www.elsevier.com/locate/optmat

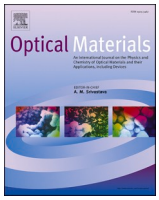

Research Article

Theoretical investigation of optical properties of optimal architectures of magnetoplasmonic nanoparticles in human tissue for potential applications in photothermal therapy

M. Hadded [a], A. Hmima [a], T. Maurer [a], A. Chehaidar [b,*], J. Plain [a]

[a] Laboratory of Light, Nanomaterials & Nanotechnologies, University of Technology of Troyes, CNRS ERL 7004, 12 Rue Marie Curie, 10000, Troyes, France
[b] University of Sfax, Faculty of Sciences of Sfax, Department of Physics, P.O.Box 1171, 3000, Sfax, Tunisia

ARTICLE INFO

Keywords:
Optical properties
Magnetoplasmonic nanoparticles
Light absorption
Light scattering
Photothermal therapy
Modeling and simulation

ABSTRACT

The absorption and scattering efficiencies of light by a single magnetoplasmonic nanoparticle, based on magnetite and gold, embedded in human tissue are analyzed theoretically in the framework of Finite-Difference-Time-Domain method and Lorenz-Mie theory. We consider separately three different architectures for the magnetoplasmonic nanoparticle: rectangular three-layer gold/magnetite/gold nanobar, circular three-layer gold/magnetite/gold nanoring and magnetite/gold core/shell nanosphere. We address the influence of particle sizes and magnetite-layer and gold-layer thicknesses on the optical response of such nanostructures. Particular attention is paid to the effectiveness of these designed nanostructures in photothermal therapy. Our simulation shows that these hybrid nanostructures support the famous localized surface plasmon resonance mode of gold, which manifests itself in the absorption spectrum by an intense peak whose spectral position can be adjusted to be in the first and second NIR-biological windows. The magnitude of the resonant absorption peak as well as that of the corresponding scattering peak vary from one nanostructure to another and, for the same nanostructure, change with its characteristic sizes. The three-layer nanobars as well as the three-layer nanorings can support significant absorption accompanied by significant scattering of light into both NIR-biological windows. For core/shell nanospheres, the low scattering efficiency of light within the second NIR-biological window, together with their large sizes, limit the usefulness of these nanostructures in photothermal therapy operating in the first NIR-biological window only.

1. Introduction

Nanoparticles continue to attract more and more attention from researchers worldwide, because of their peculiar physico-chemical properties, and especially because of their wide range of potential applications.

The properties of nanoparticles are critically dependent on their morphology, size and material composition. The optical properties of nanoparticles, in particular, have aroused particular interest from physicists as well as technologists. This interest is due to their unique properties, in particular significant enhancements of the electromagnetic field resulting in a strong scattering and absorption of light. These optical resonances have paved the way for many applications based on scattering and/or absorption of light [1–6]. Among these applications we distinguish the photothermal therapy used in cancer medicine to destroy cancer cells [7–10]. This application is based on a class of noble metal nanoparticles called plasmonic nanoparticles. These metallic particles are distinguished by their conduction electrons assimilated to a free electron gas. Excited by light, the free electrons at the surface undergo collective oscillations at specific frequencies called resonant frequencies. A resonant collective oscillation of free electrons on the nanoparticle surface is called localized surface plasmon resonance (LSPR). These resonances result in strong extinction of the light (absorption and scattering). The part of electromagnetic energy absorbed by the metallic nanoparticle is converted into heat by the Joule effect; the illuminated plasmonic nanoparticle is then assimilated to a point source of heat. Inserted into human tissue, the plasmonic nanoparticle illuminated at a given LSPR frequency causes the diseased cell to burn and therefore its destruction.

Many experimental studies have shown that gold nanoparticles are

* Corresponding author.
E-mail address: Abdallah.Chehaidar@fss.rnu.tn (A. Chehaidar).

https://doi.org/10.1016/j.optmat.2021.110946
Received 30 December 2020; Received in revised form 15 February 2021; Accepted 16 February 2021
Available online 25 February 2021

promising and typical noble metal photothermal agents [11–18]. Five types of gold nanoparticles were synthesized and entered the preclinical testing phase, namely gold nanorods [11,12], gold nanospheres [13], gold nanoshells [14], gold nanocages [15,16] and gold nanostars [17, 18]. These findings have stimulated numerous theoretical studies dedicated to the design of gold-based plasmonic nanoparticles that best meet the optimal requirements of the PTT technique and also at an affordable cost [19–27]. The dominant idea in these works is to design a hybrid nanostructure made up of gold and metallic, dielectric or magnetic material. A nanoparticle composed of gold and magnetic material is called a gold-based magnetoplasmonic nanoparticle. To our knowledge, the only structural models conceived for this kind of nanoparticles are of the core-magnetic/shell-plasmonic type cut in spherical, ellipsoidal and nanorod shapes [25–27].

In our present work, we propose other structural models for magnetoplasmonic nanoparticles formed by a layer of magnetite sandwiched between two gold layers (gold/magnetite/gold) and cut in the form of rectangular nanobar and circular nanoring. We are also re-examining the spherical Fe_3O_4/Au core/shell nanostructure. We analyze numerically the light absorption and scattering efficiencies of an individual magnetoplasmonic nanoparticle embedded in human tissue in the absence of an external static magnetic field. We address the influence of particle sizes and magnetite-layer and gold-layer thicknesses on the scattering and absorption cross-sections of such nanostructures. In addition, we discuss the efficacy of these nanoparticles in photothermal therapy.

2. Structural design and calculation method

In our present study, we are interested in the optical response of a single nanoparticle embedded in human tissue irradiated by a light wave, as illustrated schematically in Fig. 1 (a). The host medium is assumed to be unbounded and non-absorbent, and the light wave is assimilated to a plane electromagnetic wave polarized along *x*-axis and propagating along the *z*-axis. We are interested in hybrid nanoparticles composed of two different materials, one of which is magnetic such as magnetite (Fe_3O_4) and the other a noble metal such as gold (Au). In addition, we have limited ourselves to relatively simple model nanostructures, namely rectangular nanobars, circular nanorings with rectangular cross-section, and nanospheres; a schematic representation of the different nanostructures is shown in Fig. 1(b). The three-layer Au/Fe3O4/Au nanobars are characterized by a length ℓ, a width w, a gold-layer thickness $t_1$and a magnetite-layer thickness t_2. Au/Fe3O4/Au nanorings with three concentric layers are characterized by an internal radius r_1, an external radius r_2, a magnetite-layer thickness $t_1$and a gold-layer thickness t_2. Concentric core/shell nanospheres are characterized by a core radius $r_1$and a global particle radius r_2.

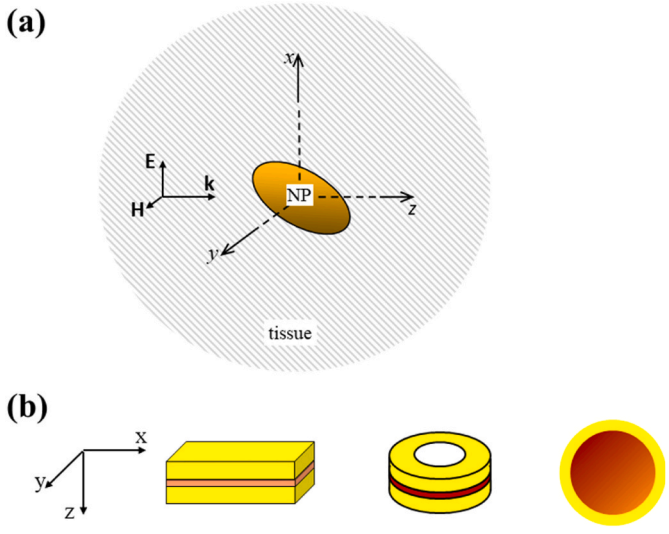

Fig. 1. (a) Schematic representation of the problem of scattering and absorption of light by a nanoparticle embedded in human tissue. **(b)** Drawings of the three gold-magnetite magnetoplasmonic nanostructures considered in the present study: three-layer Au/Fe_3O_4/Au rectangular nanobar (left), three-layer Au/Fe_3O_4/Au circular nanoring (middle) and Fe_3O_4/Au core/shell nanosphere (right).

The optical response of the nanoparticle is characterized by two dimensionless quantities, so-called scattering efficiency Q_{sca} and absorption efficiency Q_{abs}. These two quantities represent, respectively, the total electromagnetic power scattered in all the space outside the nanoparticle and that absorbed by the material constituting the nanoparticle, divided by its geometric cross-section normal to the direction of propagation of the incident light. The problem then consists in solving the famous Maxwell's equations in electric field $\vec{E}$ and magnetic field $\vec{H}$ at any point in space, taking into account the passage relations or even the continuity relations at the interfaces.

For a spherical nanoparticle an analytical solution of Maxwell's equations is available thanks to the theory of Lorenz-Mie well documented in the book of Bohren and Huffman [28]. According to this theory the scattering and absorption efficiencies of light by a spherical nanoshell are given by Ref. [28]:

$$Q_{sca} = \frac{2}{x^2}\sum_{n=1}^{\infty}(2n+1)\left(|a_n|^2+|b_n|^2\right) \quad (1)$$

$$Q_{abs} = \frac{2}{x^2}\sum_{n=1}^{\infty}(2n+1)\Re e(a_n+b_n) - Q_{sca} \quad (2)$$

where $\Re$edenotes the real part of a complex quantity, $a_n$and b_n are the Mie coefficients, and $x = 2\pi r_2/\lambda$ is the size parameter at wavelength λ. The theoretical expressions of the Mie coefficients for a spherical core/shell nanoparticle embedded in a non-absorbent matrix are developed in our recent work [23]. Using commercial MATLAB software, we have computed numerically the Mie coefficients and hence the scattering and absorption efficiencies. For nanobar and nanoring shaped nanoparticles, an analytical solution of Maxwell's equations is unfortunately not available; numerical methods are then used. In our present investigation, we have used the Finite-Difference-Time-Domain method (FDTD) [29] integrated in the commercial Lumerical software.

3. Results and discussion

The simulation of the absorption and scattering efficiencies of light by the nanostructures under consideration requires as input data the complex refractive indices as well as the permeabilities of the various component materials, namely surrounding medium, gold and magnetite. As we mentioned before, human tissue is assumed to be a non-absorbent medium, which amounts to assigning it a pure real refractive index. In reality, this approximation is not valid for the whole electromagnetic spectrum, but it does apply in a few intervals, in particular in the wavelength ranges 650 − 950 nmand 1000 − 1350 nmcalled first and second biological Near-Infrared windows [30]. Experimental measurements have shown that the refractive index of human tissue disperses little in the optical domain. In our calculations we have taken a single value of 1.44 [31] along the wavelength range under consideration. Values of the complex refractive indices measured for bulk crystalline Fe_3O_4 [32], and bulk crystalline gold [33] were used. The missing data were interpolated from the available experimental data by cubic spline interpolation method. For gold, the complex refractive index was corrected for the nanoparticle size [34]. The refractive indices n and the extinction coefficients κ for the materials considered here are shown as curves in Fig. 2 over the 200–1400 nm wavelengths range. The surrounding medium and gold are non-magnetic in nature, and thus have the same permeability as vacuum. Magnetite on the other hand is a

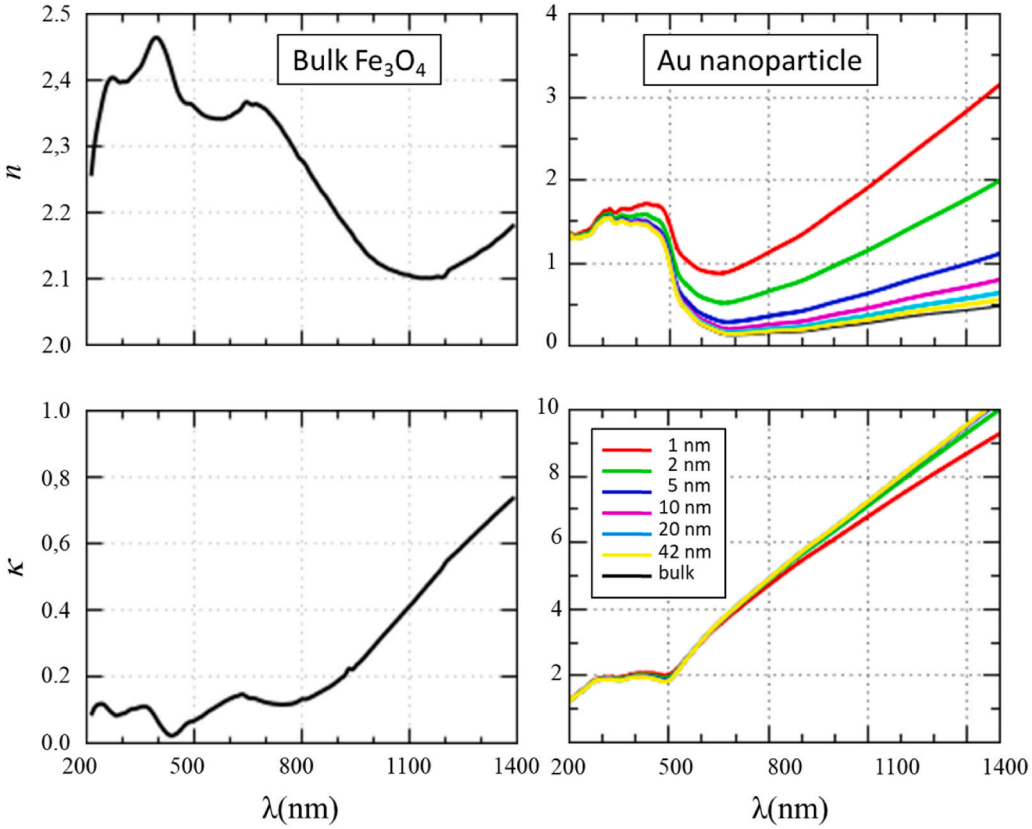

Fig. 2. The refractive index n and the extinction coefficient κ of bulk Fe_3O_4 (left), and gold nanoparticle (right).

magnetic material, and its magnetism manifests itself in the presence of an applied magnetic field and also in the low frequency range. In our case, the applied magnetic field of the incident light is extremely weak and in addition acts in the high frequency domain (the optical domain). Thus, we have assumed that the permeability of magnetite is the same as that of vacuum.

Besides the optical properties of the materials composing the target nanoparticle, the simulation of its optical response also requires its characteristic sizes as input data. Remember that the main objective of our simulations is to determine the characteristic sizes of the proposed nanostructures giving rise to resonant absorptions of light in the two biological NIR-windows. For core/shell nanospheres the calculation is fast thanks to the Lorenz-Mie theory. Thus, we have treated all the particle-diameters ranging from 2 to 500 nm, and all the shell-thickness fractions between 0 and 1. Regarding now the three-layer $Au/Fe_3O_4/Au$ nanostructures, the calculations are carried out by the numerical FDTD method which is time-consuming, and it is therefore necessary to select a few sizes. In any case, the sizes of these nanoparticles should not exceed 100 nm to facilitate their penetration into human tissues. For the $Au/Fe_3O_4/Au$ nanobars, we started with the sizes of the pure gold nanobars previously reported by Ghosh et al. [21], namely a length of 100 nm, a width of 60 nm and a thickness of 10 nm. We then examined the effect of the aspect ratio defined by the length/width ratio, and furthermore the effect of the thicknesses of the gold layer and of the magnetite layer; here it should be noted that we have limited ourselves to gold-layer thicknesses of less than 10 nm because we are seeking to reduce the cost of the nanostructures in question. Regarding now $Au/Fe_3O_4/Au$ nanorings, the choice of the overall size is in fact arbitrary but must not exceed 100 nm, as mentioned above.

The results of our simulations will now be presented and discussed. We start with the three-layer $Au/Fe_3O_4/Au$ nanobars, then the three-layer $Au/Fe_3O_4/Au$ nanorings and finally the Fe_3O_4/Au core/shell nanospheres.

3.1. *Three-layer $Au/Fe_3O_4/Au$ nanobars*

We started by computing the absorption spectra of pure gold nanobars to ensure the proper functioning of our FDTD code. Fig. 3 shows the results of our FDTD calculations for gold nanobars of length 100 nm, width 60 nmand different thicknesses t (between 8 and 60 nm) embedded in a homogeneous medium of refractive index 1.25. As can be seen from this figure, our FDTD simulation well reproduces the results reported by Ghosh et al. [21] using the finite element method. As expected, the spectra show a resonant absorption peak attributed to the LSPR mode of gold. For a perfect rectangular nanobar, this peak is found to shift from the visible towards the NIR by reducing its thickness; more

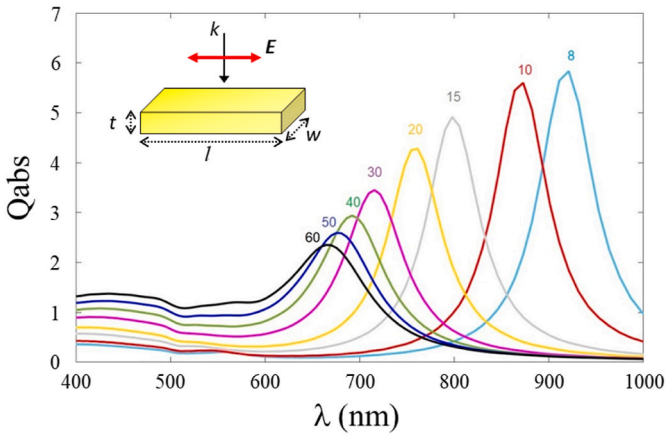

Fig. 3. Computed absorption spectra for gold nanobars of width $w = 60$ nm, length $\ell = 100$ nm and various thicknesses t embedded in homogeneous medium of refractive index 1.25; the computation is performed using FDTD method.

quantitatively, it shifts from 600 nmfor $t = 60$ nmto 980 nmfor $t = 8$ nm. In addition, its magnitude is also thickness dependent where it increases while decreasing the thickness for a fixed length and width; more quantitatively, the maximum absorption efficiency of ~3 for $t =$ 60 nm jumps to the value ~7 for $t = 8$ nm.

The scattering and absorption spectra simulated for three-layer Au/Fe_3O_4/Au nanobars, 100 nm long and 60 nm wide, embedded in human tissue, are shown in Fig. 4. The results relate to six nanobars, three of which have a gold layer of thickness 5 nm and the other three have a gold layer 10 nm thick; for each gold layer thickness, three thicknesses of the magnetite layer were considered: 10, 20 and 30 nm. For comparison, this figure also shows the scattering and absorption spectra of pure gold nanobars of thicknesses 5 and 10 nm. The Q_{sca} and Q_{abs} spectra of the Au/Fe_3O_4/Au three-layer nanobar have the same shape as those of a pure gold nanobar; they are dominated by the LSPR peak of gold. The spectral position, magnitude and linewidth of the LSPR peak in Au/Fe_3O_4/Au three-layer nanobars differ from those relating to the LSPR peak in pure gold, and are dependent on the thickness of the magnetite separation layer. The spectral shift of the LSPR peak in the sandwich nanobar with respect to its counterpart in the gold nanobar is manifested in both directions. A blue shift occurs for a magnetite layer of thickness less than 20 nm practically, and a red shift for greater thicknesses. The linewidth of the LSPR peak is found to increase by increasing the thickness of the magnetite layer. In absorption, the intensity of the LSPR peak in the Au/Fe_3O_4/Au nanobar can never exceed that of the LSPR peak in the monolayer-gold nanobar. It can be, however, in the light scattering; this opportunity is achieved with a very thin magnetite separation layer. At this level, one may wonder if rectangular nanobars, whether pure gold or three-layer Au/Fe_3O_4/Au, are effective in PTT whatever the thickness of the gold layer. Here it must be remembered that PTT requires plasmonic agents with high NIR light absorption efficiency to effectively burn cancer cells, but at the same time these agents must be good light scatterers in order to be able to image the target cells or tissues before, during and after the therapy. According to Fig. 4, this requirement rules out nanobars with gold layers of thicknesses smaller than 10 nm. In this context, we can also affirm the superiority of three-layer Au/Fe_3O_4/Au nanobars over pure gold nanobars.

We now turn our attention to the effect of the aspect ratio, defined as the length to width ratio (ℓ/w), on the spectra of the absorption and scattering efficiencies of a rectangular nanobar embedded in human tissue. We have thus examined two sets of rectangular nanobars with predefined thicknesses of the gold and magnetite layers. For the first set, we have fixed the width at 60 nm and vary the length between 60 and 100 nm by a step of 20 nm. For the second, it is the length which is fixed (at 100 nm) but the width varies between 10 and 60 nm by a step of 10 nm. The results of our simulations are reported in Fig. 5 for three-layer Au/Fe_3O_4/Au nanobars having a gold-layer thickness of 10 nm and a magnetite-layer thickness of 20 nm. It is clear from this figure that the LSPR peak strongly depends on the aspect ratio of the nanobar. For a fixed width w at 60 nm, the LSPR peak in three-layer Au/Fe_3O_4/Au nanobar blushifts and its magnitude decreases by decreasing its length from $\ell = 100$ nm to $\ell = w$. Now, for a fixed length ℓ at 100 nm, the LSPR peak of the Au/Fe_3O_4/Au nanobar redshifts remarkably with a magnitude which increases in absorption but decreases in scattering when the width w decreases from 60 to 10 nm. Although the 100 nm long and 10 and 20 nm wide nanobars are good light absorbers, they are unfortunately not suitable for PTT, as they weakly scatter light and therefore do not allow imaging. Nanobars with widths between 30 and 60 nm absorb light less effectively than the previous ones, but on the other hand, they scatter light better and therefore are more suitable for PTT. The linewidth of the LSPR peak seems to be insensitive to the aspect ratio of the nanobar.

3.2. *Three-layer Au/Fe_3O_4/Au nanorings*

We now move on to the second type of nanostructures proposed in this work, namely circular three-layer Au/Fe_3O_4/Au nanorings. Remember that the two layers of gold have the same thickness. In Fig. 6

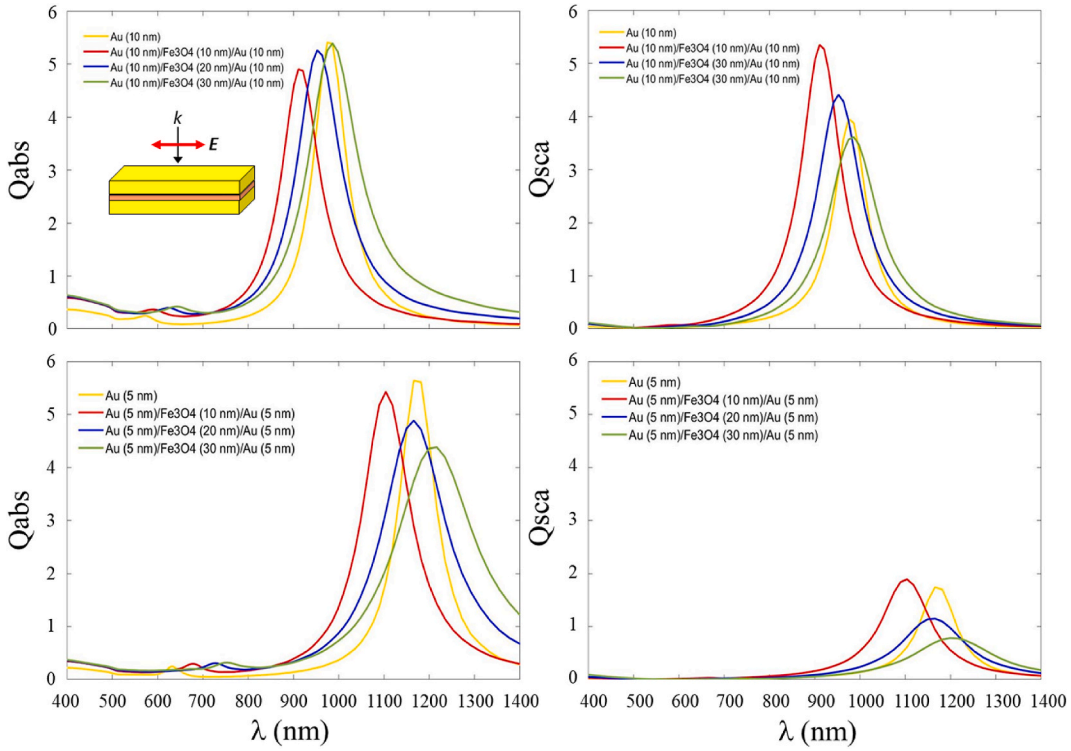

Fig. 4. Computed absorption and scattering spectra for a single three-layer Au/Fe_3O_4/Au nanobar embedded in human tissue with gold-layer thickness of 10 nm (top panels) and 5 nm (lower panels) and different magnetite-layer thicknesses. The length and the width of the rectangular nanobar are maintained fix at 100 and 60 nm, respectively.

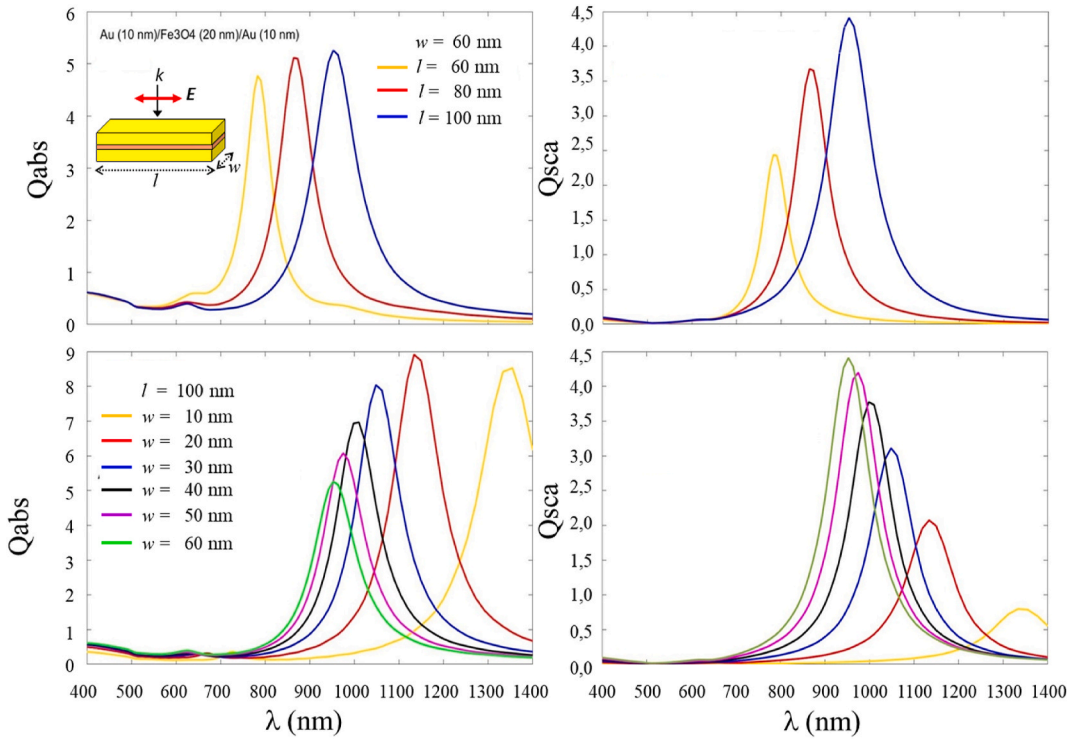

Fig. 5. Computed absorption and scattering efficiency spectra for a single three-layer Au/Fe_3O_4/Au nanobar embedded in human tissue for different aspect ratios ℓ/w: (top panels) the width w is set at 60 nm, (lower panels) the length ℓ is set at 100 nm. The gold-layer and the magnetite-layer thicknesses are set at 10 and 20 nm, respectively.

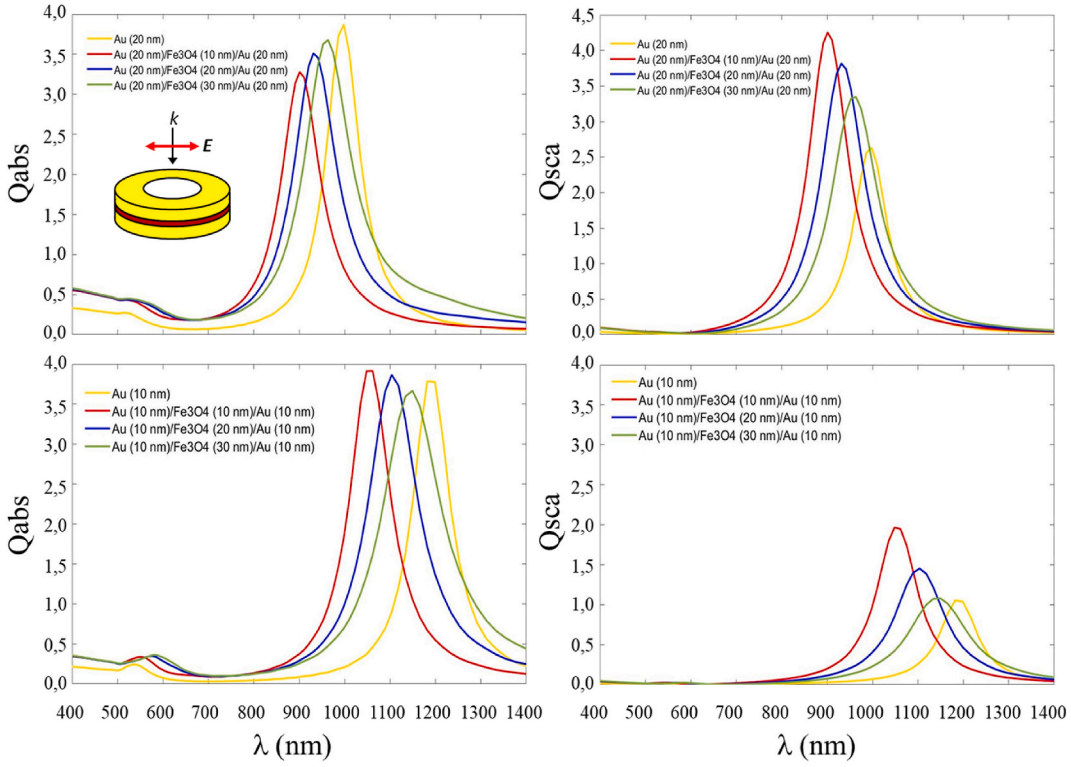

Fig. 6. Computed absorption and scattering spectra for a single three-layer Au/Fe_3O_4/Au nanoring embedded in human tissue with gold-layer thickness of 20 nm (top panels) and 10 nm (lower panels) and different magnetite-layer thicknesses. The internal and external radii of the nanoring are set at 30 and 50 nm, respectively.

we expose the light absorption and scattering efficiency spectra computed for two sets of nanorings having as common characteristics an internal radius $r_1 = 30$ nm and an external radius $r_2 = 50$ nm: the first set is formed by nanorings having a gold layer 5 nm thick and a magnetite layer 10, 20 and 30 nm thick; the second set is formed by nanorings having a gold layer 10 nm thick and a magnetite layer 10, 20

and 30 nm thick. For comparison, this figure also shows the spectra computed for pure gold nanorings. The optical spectra of Au/Fe_3O_4/Au nanoring have the same overall appearance as those relating to pure gold nanoring; they are dominated by the LSPR peak of gold. Three-layer nanorings are able to absorb light along the optical domain and more specifically in the first and second biological NIR windows. The spectral position, magnitude and linewidth of the LSPR peak in three-layer Au/Fe_3O_4/Au nanorings differ from those relating to the LSPR peak in pure gold nanoring, and are dependent on the thickness of the magnetite separation layer. The spectral shift of the LSPR peak in the sandwich nanoring with respect to its counterpart in the pure gold nanoring is manifested towards blue regardless of the thickness of the gold layers and for the thickness values of the magnetite-layer considered here. It is almost zero for 50 nm thick magnetite layer and increases monotically with increasingly thin ones. For sandwich nanorings with gold layers of thicknesses 10 and 20 nm, the magnitude of the absorption efficiency is almost identical to that corresponding to pure gold nanorings, while the magnitude of the scattering efficiency is much improved, especially with very thin magnetite layers. It should be noted that the light scattering efficiency by Au/Fe_3O_4/Au nanorings with 10 nm thick gold layers is low compared to that of nanorings with thicker gold layers. For nanorings with gold layers 5 nm thick, the magnitude of the scattering efficiency is worse; in the best case it does not exceed the value 0.1. The linewidth of the LSPR peak is found to increase by increasing the thickness of the manganite layer.

In addition to the thicknesses of the gold and magnetite layers, the nanoring provides additional geometric parameters namely its internal and external radii (r_1 and r_2, respectively), also allowing the adjustment of the characteristics of the LSPR peak. Indeed, this is what can be seen in Fig. 7 showing absorption and scattering efficiency spectra computed for two sets of Au/Fe_3O_4/Au nanorings having layers of gold and magnetite 10 nm thick, an external radius $r_2 = 25$ nm for the first set and 50 nm for the second, but different values for the internal radius r_1. It is important to note from this figure, that the small nanorings can be good absorbers of NIR light but they are poor scatteres of this light; the larger nanorings, on the other hand, can be both good absorbers and scatteres of NIR light. In addition, we note the wide spectral margin, going from visible to mid-infrared, offered by the variation of the internal radius of the nanoring. However, the requirement of efficient absorption and efficient scattering of NIR light in PTT limits the choice of inner and outer radii to few values. In this context, nanorings with an external radius of 25 nm are discarded, and among the nanorings with an external radius of 50 nm only the one with an internal radius of 20 nm seems to be the most suitable.

3.3. Fe_3O_4/Au core/shell nanospheres

As mentioned above, the optical response of Fe_3O_4/Au core/shell nanospheres in an aqueous medium has been theoretically investigated by Brullo et al. [26] and Hadilou et al. [27]. None of these works reported absorption in the second biological NIR-window, which seems a bit strange to us. So we reconsider here this type of nanostructure and we analyze by Lorenz-Mie theory its optical response for wider ranges of particle diameter and shell thickness.

The absorption and scattering efficiencies of a single Fe_3O_4/Au core/shell spherical nanoparticle embedded in human tissue are plotted in two-dimensional color maps as function of the outer diameter $D(=2r_2)$, the vacuum wavelength λ, and for different gold-shell thickness fractions $t_f(=(r_2-r_1)/r_2)$. The results obtained for $t_f = 0.1$, 0.25 and 0.5 are shown in Fig. 8. For comparison, results for pure gold nanosphere are also shown in this figure. Our simulation results are given for particle diameters in the 2–400 nm range and for wavelengths in the 200–1400 nm range.

A global observation of these color maps shows that Fe_3O_4/Au core/shell nanospheres differ from pure gold nanospheres, with respect to absorption and scattering of light, only for gold-shell thickness fractions $t_f$less than 0.5. In addition, this difference becomes more and more obvious with increasingly small shell thickness fractions. A detailed

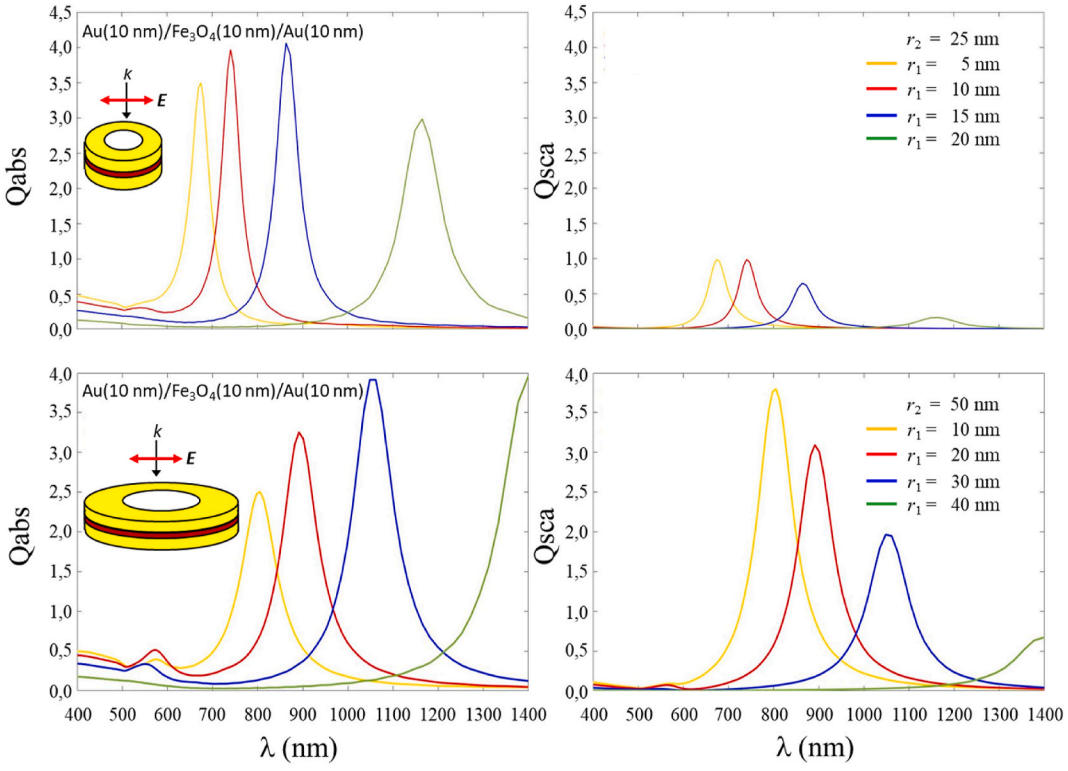

Fig. 7. Computed absorption and scattering efficiency spectra for a single three-layer Au/Fe_3O_4/Au nanoring embedded in human tissue with external radii of 25 nm (top panels) and 50 nm (lower panels) and different internal radii. The gold-layer and the magnetite-layer thicknesses are set at 10 nm.

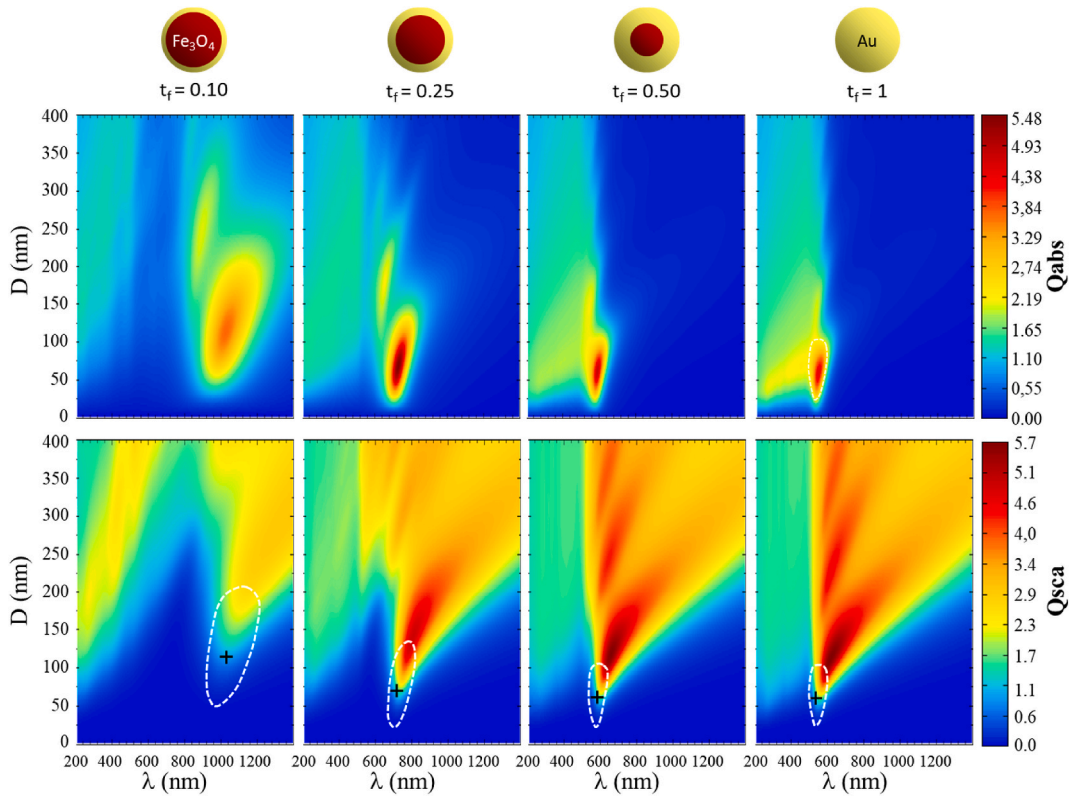

Fig. 8. The absorption efficiency Q_{abs} (top) and scattering efficiency Q_{sca} (bottom) of a single Fe_3O_4/Au core/shell nanosphere embedded in human tissue, as a function of the nanoparticle diameter D, the incident light wavelength λ, and for different shell thickness fractions t_f. The white dashed line added to the *Qsca* color map represents the outline of the corresponding resonant absorption branch, and the black cross identifies the mode at its barycenter.

observation of these maps shows that the pure gold nanosphere exhibits a resonant absorption corresponding to the LSPR located in the range of wavelengths 520–580 nm for particle diameters in the range 40–80 nm. The optimal absorption resonance is centered on $\lambda = 544$ nmand corresponds to particle diameter $D = 60$ nm. It should be noted that the useful absorption spectral range of pure gold nanosphere is located in the visible range where the phenomena of light absorption by the constituents of human tissue are manifested. Now for the core/shell nanospheres with a gold-shell thickness fraction $t_f < 0.5$, the Q_{abs} color maps highlight absorption resonances in the spectral domain where the gold particle does not absorb; precisely, beyond 600 nm. These resonant modes form a diffuse branch in the wavelength-diameter plane. The distribution of the magnitude of the resonance modes on the branch is not uniform; it is maximum in the barycenter of the branch and gradually decreases towards its edges. Such branch covers a finite spectral domain, and manifests itself in a finite range of particle sizes as well. For $t_f = 0.25$ for example, this branch is spread over the 700–800 nm wavelength range and the 25–125 nm diameter range, with a barycenter located at $\lambda = 729$ nm and a particle diameter $D = 70$ nm. By decreasing the gold-shell thickness fraction, this branch redshifts and at the same time pushes slightly towards larger particle diameters. More quantitatively, for $t_f = 0.1$, this branch covers the 960–1120 nm wavelength range and the 50–200 nm diameter range, with a barycenter located at $\lambda = 1028$ nm and a particle diameter $D = 116$ nm.

As can be seen from the available maps shown in Fig. 8, the maximum absorption efficiency at the barycenter of a branch depends on the gold-shell thickness fraction t_f. This observation is made clearer in Fig. 9 showing the absorption efficiency spectra computed for the Fe_3O_4-core/Au-shell nanospheres supporting the resonance modes at the barycentres of the branches for gold-shell thickness fractions ranging from 0.05 to 0.4 in a step of 0.05. From this figure, it can also be noted that the Fe_3O_4/Au core/shell nanospheres embedded in human tissue

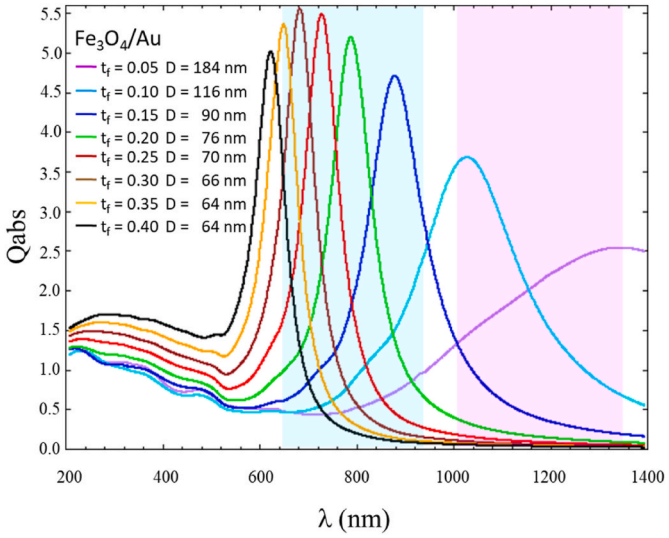

Fig. 9. Computed absorption efficiency spectra for a single Fe_3O_4/Au nanosphere embedded in human tissue, supporting the most intense resonance mode for different gold-shell thickness fractions t_f. The shaded areas delimit the first (in cyan) and the second (in pink) biological NIR-windows.

are capable of absorbing light in the two biological NIR-windows. The first biological window involves nanospheres with a gold-shell thickness fraction $t_f$of between 0.35 and 0.125 and a particle diameter D of between 25 and 190 nm, while the second window corresponds to $t_f$of between 0.1 and 0.05 and a particle diameter D of between 70 and 300 nm. If we now come back to the overall sizes and shell thicknesses of Fe_3O_4/Au core/shell nanospheres considered in the works of Brullo et al.

[26] and Hadilou et al. [27], we clearly understand why they did not report absorption resonances in the second biological NIR-window. It is also important to note from the shape of the absorption spectra reported in Fig. 9, that the absorption of light in the first biological NIR-window is selective and works well with near monochromatic sources, while that in the second window spreads out over a wide spectral band and is therefore suitable with polychromatic sources. So far, Fe_3O_4/Au core/-shell nanospheres appear to be effective in PTT. It now remains to see their light scattering efficiency, part of which is absorbed by the nanoparticle in question. For this, we had the idea of superimposing on each Q_{sca} color map the hand-drawn outline of the corresponding absorption resonance branch (shown in dashed white line) as well as its barycenter (reported by a black cross). It can be seen that the lower half of the resonant absorption branch corresponds to a virtually zero scattering efficiency. On the other hand, the upper half of the absorption branch, including the optimum mode at the barycenter, is associated with resonant scattering modes. The magnitude of these resonant scattering modes is low at the barycenter of the absorption branch, and gradually increases away from this towards large diameters. Thus, our simulation highlights a threshold size for each gold-shell thickness fraction below which the Fe3O4-core/Au-shell nanospheres do not scatter NIR light and therefore do not operate in PTT coupled with imaging. This threshold size corresponds to the absorption mode at the barycenter of the resonant absorption branch. More quantitatively, the threshold sizes evaluated for the thickness fractions examined in our present work are reported in Fig. 9. We can then deduce that the Fe_3O_4-core/Au-shell nanospheres operating in the second biological NIR-window must be much larger than 100 nm, thus greatly exceeding the optimal sizes (10–100 nm) used in PTT of cancer cells [35].

4. Conclusion

In this paper we have presented the results of numerical simulations of light absorption and scattering efficiencies by a magnetoplasmonic nanoparticle, based on magnetite and gold, embedded in human tissue, intended to be used as PTT agents. Three different architectures have been considered for the magnetoplasmonic nanoparticle: rectangular three-layer Au/Fe_3O_4/Au nanobar, circular three-layer Au/Fe_3O_4/Au nanoring and Fe_3O_4/Au core/shell nanosphere. Our simulation shows that these hybrid nanostructures support the famous LSPR mode of gold, which is reflected in the absorption spectrum by an intense peak whose spectral position can be adjusted to be in the first and second biological NIR-windows. The magnitude of the resonant absorption peak as well as that of the corresponding scattering peak vary from one nanostructure to another and, for the same nanostructure, change with its characteristic sizes. The three-layer nanobars as well as the three-layer nanorings can support significant absorption accompanied by significant scattering of light into both biological NIR-windows with a largest characteristic size not exceeding 100 nm. Significant scattering of NIR light accompanying significant resonant absorption by the core/shell nanospheres is much less evident than in the previous two cases, especially in the second NIR-biological window where the useful size of the nanoparticle exceeds the optimal sizes used in PTT. We are thus making available to the scientific and technological communities, two new magnetoplasmonic nanostructures that prove to be potential candidates for application in PTT therapy coupled with imaging and operating efficiently in both biological NIR-windows.

Author contribution

Maha Hadded: Plain have contributed equally to this work. Abdelhamid Hmima: Plain have contributed equally to this work. Thomas Maurer: Plain have contributed equally to this work. Abdallah Chehaidar: Plain have contributed equally to this work. Jérôme Plain: have contributed equally to this work.

Declaration of competing interest

The authors declare that they have no known competing financial interests or personal relationships that could have appeared to influence the work reported in this paper.

References

[1] O.V. Salata, Applications of nanoparticles in biology and medicine, J. Nanobiotechnol. 2 (2004) 3, https://doi.org/10.1186/1477-3155-2-3.

[2] Q. Rehman, A.D. Khan, A.D. Khan, M. Noman, H. Ali, A. Rauf, M.S. Ahmad, Super absorption of solar energy using a plasmonic nanoparticle based CdTe solar cell, RSC Adv. 9 (2019) 34207–34213, https://doi.org/10.1039/C9RA07782K.

[3] E. Tiguntseva, et al., Resonant silicon nanoparticles for enhancement of light absorption and photoluminescence from hybrid perovskite films and metasurfaces, Nanoscale 9 (2017) 12486–12493, https://doi.org/10.1039/c7nr01631j.

[4] N. Serpone, R.F. Khairutdinov, Application of nanoparticles in the photocatalytic degradation of water pollutants, in: Studies in Surface Science and Catalysis, vol. 103, 1997, pp. 417–444.

[5] J.-R. Choi, D.-M. Shin, H. Song, D. Lee, K. Kim, Current achievements of nanoparticle applications in developing optical sensing and imaging techniques, Nano Converg. 3 (2016) 30–42, https://doi.org/10.1186/s40580-016-0090-x.

[6] T. Thuy Nguyen, F. Mammeri, S. Ammar, Iron oxide and gold based magneto-plasmonic nanostructures for medical applications: a review, Nanomaterials 8 (2018) 149–177, https://doi.org/10.3390/nano8030149.

[7] D. Jaque, L. Martinez Maestro, B. del Rosal, P. Haro-Gonzalez, A. Benayas, J. L. Plaza, E. Martin Rodriguez, J. Garcia Solé, "Nanoparticles for photothermal therapies,", Nanoscale 6 (2014) 9494–9530, https://doi.org/10.1039/c4nr00708e.

[8] N.S. Abadeer, C.J. Murphy, Recent progress in cancer thermal therapy using gold nanoparticles, J. Phys. Chem. C 120 (2016) 4691–4716, https://doi.org/10.1021/acs.jpcc.5b11232.

[9] C. Multari, M. Miola, F. Laviano, R. Gerbaldo, G. Pezzotti, D. Debellis, E. Verné, Magnetoplasmonic nanoparticles for photothermal therapy, Nanotechnology 30 (2019) 255705–255713, https://doi.org/10.1088/1361-6528/ab08f7.

[10] W. Yang, H. Liang, S. Ma, D. Wang, J. Huang, Gold nanoparticle based photothermal therapy: development and application for effective cancer treatment, Sustain. Mater. Technol. 22 (2019), e00109, https://doi.org/10.1016/j.susmat.2019.e00109.

[11] Y.-Y. Yu, S.-S. Chang, C.-L. Lee, C.C. Wang, Gold nanorods: electrochemical synthesis and optical properties, J. Phys. Chem. B 101 (1997) 6661–6664.

[12] F. Kim, J.H. Song, P. Yang, Photochemical synthesis of gold nanorods, J. Am. Chem. Soc. 124 (2002) 14316–14317.

[13] A.M. Schwartzberg, T.Y. Olson, C.E. Talley, J.Z. Zhang, Synthesis, characterization, and tunable optical properties of hollow gold nanospheres, J. Phys. Chem. B 110 (2006) 19935–19944, https://doi.org/10.1021/jp062136a.

[14] B. Storti, F. Elisei, S. Abbruzzetti, C. Viappiani, L. Latterini, One-pot synthesis of gold nanoshells with high photon-to-heat conversion efficiency, J. Phys. Chem. C 113 (2009) 7516–7521, https://doi.org/10.1021/jp810544b.

[15] S.E. Skrabalak, J. Chen, Y. Sun, X. Lu, L. Au, C.M. Cobley, Y. Xia, Gold nanocages: synthesis, properties, and applications, Acc. Chem. Res. 41 (2008) 1587–1595, https://doi.org/10.1021/ar800018v.

[16] Y. Xia, W. Li, C.M. Cobley, J. Chen, X. Xia, Q. Zhang, M. Yang, E.C. Cho, P. K. Brown, Gold nanocages: from synthesis to theranostic applications, Acc. Chem. Res. 44 (2011) 914–924, https://doi.org/10.1021/ar200061q.

[17] P.S. Kumar, I. Pastoriza-Santos, B. Rodriguez-Gonzalez, F.J.G. De Abajo, L.M. Liz-Marzan, High-yield synthesis and optical response of gold nanostars, Nanotechnology 19 (2007), https://doi.org/10.1088/0957-4484/19/01/015606, 015606-015611.

[18] Y. Liu, J.R. Ashton, E.J. Moding, H. Yuan, J.K. Register, A.M. Fales, J. Choi, M. J. Whitley, X. Zhao, Y. Qi, Y. Ma, G. Vaidyanathan, M.R. Zalutsky, D.G. Kirsch, C. T. Badea, T. Vi-Dinh, A plasmonic gold nanostar thernostic probe fir *in vivo* tumor imaging and photothermal therapy, Theranostics 5 (2015) 946–960, https://doi.org/10.7150/thne.11974.

[19] M.-F. Tsai, S.-H. Gilbert Chang, F.-Y. Cheng, V. Shanmugam, Y.-S. Cheng, C.-H. Su, C.-S. Yeh, Au nanorod design as light-absorber in the first and second biological Near-Infrared windows for *in vivo* photothermal therapy, ACS Nano 7 (2013) 5330–5342, https://doi.org/10.1021/nn401187c.

[20] D. Sikdar, I.D. Rukhlenko, W. Cheng, M. Premaratne, Effect of number density on optimal design of gold nanoshells for plasmonic photothermal therapy, Biomed. Optic Express 4 (2013) 15–31.

[21] P.K. Ghosh, D.T. Debu, D.A. French, J.B. Herzog, Calculated thickness dependent plasmonic properties of gold nanobars in the visible to near-infrared light regime, PLoS One 12 (2017), e0177463, https://doi.org/10.1371/journal.pone.0177463.

[22] P. Tuersun, X. Yakupu, X.E. Han, Y. Yin, Optimization of nonspherical gold nanoparticles for photothermal therapy, Appl. Sci. 9 (2019) 4300–4307, https://doi.org/10.3390/app9204300.

[23] A. Chehaidar, M. Hadded, Scattering and absorption of light by homogeneous BiFeO3 and hybrid BiFeO3/Au core/shell spherical nanoparticles: a computational study, Opt. Mater. 95 (2019) 109207–109218, https://doi.org/10.1016/j.optmat.2019.109207.

[24] W. Chaabani, A. Chehaidar, J. Plain, A. Chehaidar, M. Hadded, Comparative theoretical study of the optical properties of slicon/gold, silica/gold core/shell and gold spherical nanoparticles, Plasmonics 11 (2016) 1525–1535, https://doi.org/10.1007/s11468-016-0206-5.

[25] X. Xue, V. Sukhotskiy, E.P. Furlani, Optimization of optical absorption of colloids of SiO_2@Au and Fe_3O_4@Au nanoparticles with constraints, Sci. Rep. 6 (2016) 35911–35920, https://doi.org/10.1038/srep35911.
[26] W. Brullot, V.K. Valev, T. Verbiest, Magnetic-plasmonic nanoparticles for the life sciences: calculated optical properties of hybrid structures, Nanomed. Nanotechnol. Biol. Med. 8 (2012) 559–568, https://doi.org/10.1016/j.nano.2011.09.004.
[27] N. Hadilou, S. Souri, H.A. Navid, R. Sadighi Bonabi, A. Anvari, B. Palpant, An optimal architecture of magneto-plasmonic core-shell nanoparticles for potential photothermal applications, Phys. Chem. Chem. Phys. 22 (2020) 14318–14328, https://doi.org/10.1039/d0cp01509a.
[28] C.F. Bohren, D.R. Huffman, Absorption and Scattering of Light by Small Particles, John Wiley & Sons, 2008.
[29] U.S. Inan, R.A. Marshall, Numerical Electromagnetics: the FDTD Method, Cambridge University Press, 2011.
[30] A.M. Smith, M.C. Mancini, S. Nie, Second window for in vivo imaging, Nat. Nanotechnol. 4 (2009) 710–711, https://doi.org/10.1038/nnano.2009.326.
[31] M.-F. Tsai, S.-H. Gilbert Chang, F.-Y. Cheng, V. Shanmugam, Y.-S. Cheng, C.-H. Su, C.-S. Yeh, Au nanorod design as light-absorber in the first and second biological near-infrared windows for in vivo photothermal therapy, ACS Nano 7 (2013) 5330–5342, https://doi.org/10.1021/nn401187c.
[32] M.R. Querry, Optical Constants, Contractor Report CRDC-CR-85034, 1985.
[33] P.B. Johnson, R.W. Christy, Optical constants of the noble metals, Phys. Rev. B 6 (1972) 4370–4379.
[34] C.L. Nehl, N.K. Grady, G.P. Goodrich, F. Tam, N.J. Halas, J.H. Hafner, Scattering spectra of single gold nanoshells, Nano Lett. 4 (2004) 2355–2359.
[35] P.C. Chen, S.C. Mwakwari, A.K. Oyelere, Gold nanoparticles: from nanomedicine to nanosensing, Nanotechnol. Sci. Appl. 1 (2008) 45–66, https://doi.org/10.2147/nsa.s3707.